**SUPPLEMENTARY MATERIAL TO THE PAPER "THE TEMPERATURE AND PRESSURE DEPENDENCE OF NICKEL PARTITIONING BETWEEN OLIVINE AND SILICATE MELT"**

**A. K. Matzen, M. B. Baker, J. R. Beckett, and E. M. Stolper.**

In this Supplement, we provide seven sections that expand and/or illustrate specific topics presented in the main text. The first section is a sample calculation using our preferred partitioning expression, equation (5), from the main text. Section 2 compares our fitted values of $-\frac{\Delta_r H^{\circ}_{T_{ref},P_{ref}}}{R}$ and $\frac{\Delta_r S^{\circ}_{T_{ref},P_{ref}}}{R}$ for equation (5) to those calculated using tabulated thermodynamic data. In Section 3, we present details of the mass-balance calculations used to evaluate the experiments from both this work and the literature, and in Section 4 we describe in detail the construction of the Filter-B dataset. Section 5 details the construction and fits of the regular solution partitioning models. Section 6 is a comparison of the results of this work and the Beattie-Jones family of models. Finally, Section 7 lists all of the references incorporated into our database on olivine-liquid Ni partitioning.

## 1. EXAMPLE CALCULATION USING OUR PREFERRED PARTITIONING EXPRESSION (EQUATION 5) FROM THE MAIN TEXT

Although one of the simplest equations listed in the text, we think it useful to present a detailed accounting of how to use equation (5) along with the fitted parameters presented in Table 4 to predict $D_{Ni}^{ol/liq}$ (where $D_{Ni}^{ol/liq}$ = $NiO^{ol}/NiO^{liq}$, by wt.) given the temperature and compositions of the coexisting olivine and liquid. In our example calculation, we predict the partition coefficient for one of our 1.0 GPa experiments, Run 6. In the following tables, liquid and olivine compositions are reported to 2 or 4 decimal places and all calculated values are reported to 4

decimal places; even though not statistically justified, we do this to allow for an easy comparison with the reader's calculations.

### 1.1 Initial Information

Temperature (K) =1723.15

Table S1. Liquid composition (wt. %)

| | |
|---|---|
| $SiO_2$ | 49.91 |
| $TiO_2$ | 1.41 |
| $Al_2O_3$ | 11.10 |
| $Cr_2O_3$ | 0.0150 |
| FeO* | 10.73 |
| MnO | 0.20 |
| MgO | 17.66 |
| CaO | 7.41 |
| $Na_2O$ | 1.95 |
| $K_2O$ | 0.1204 |
| $P_2O_5$ | 0.1120 |
| NiO | 0.0729 |

Table S2. Olivine composition (wt. %)

| | |
|---|---|
| $SiO_2$ | 40.74 |
| $TiO_2$ | 0.0223 |
| $Al_2O_3$ | 0.0703 |
| $Cr_2O_3$ | 0.0130 |
| FeO* | 9.94 |
| MnO | 0.1415 |
| MgO | 48.56 |
| CaO | 0.2128 |
| $Na_2O$ | 0 |
| $K_2O$ | 0 |
| $P_2O_5$ | 0 |
| NiO | 0.3243 |

For reference, the measured $D_{Ni}^{ol/liq}$ (using the truncated data listed above) = 4.4486

### 1.2 Transforming to molar components

Fits to the equations presented in the text are performed using mole fractions; therefore, to predict a partition coefficient it is necessary to transform each composition from weight percent

into mole fractions. Transforming the liquid composition to a molar basis is relatively straightforward (divide the wt. % values by their gram-formula weights and renormalize the moles to mole fractions). Note that for the liquid silica component we use $Si_{0.5}O$ instead of the more common $SiO_2$ in order to facilitate writing the formation reaction (see the main text).

Table S3. Liquid composition in moles and gram-formula weights

| Components | Moles | Formula weights |
|---|---|---|
| $Si_{0.5}O$ | 1.6613 | 30.04215 |
| $TiO_2$ | 0.0177 | 79.8658 |
| $Al_2O_3$ | 0.1089 | 101.9613 |
| $Cr_2O_3$ | 0.0001 | 151.9904 |
| FeO* | 0.1494 | 71.8444 |
| MnO | 0.0028 | 70.9374 |
| MgO | 0.4382 | 40.3044 |
| CaO | 0.1321 | 56.0774 |
| $Na_2O$ | 0.0315 | 61.9789 |
| $K_2O$ | 0.0013 | 94.196 |
| $P_2O_5$ | 0.0008 | 141.9445 |
| NiO | 0.0010 | 74.6928 |
| CoO | 0 | 74.9326 |

Renormalizing by the sum of the total number of moles in the liquid (2.5449) gives the liquid composition in mole fractions.

Table S4. Liquid composition expressed as mole fractions

| Components | Mole fract. |
|---|---|
| $Si_{0.5}O$ | 0.6528 |
| $TiO_2$ | 0.0069 |
| $Al_2O_3$ | 0.0428 |
| $Cr_2O_3$ | 0.0000 |
| FeO* | 0.0587 |
| MnO | 0.0011 |
| MgO | 0.1722 |
| CaO | 0.0519 |
| $Na_2O$ | 0.0124 |
| $K_2O$ | 0.0005 |
| $P_2O_5$ | 0.0003 |
| NiO | 0.0004 |
| CoO | 0 |

Transforming the olivine composition into olivine components is only slightly more involved: First, the composition in wt. % is transformed into moles and mole fractions of the oxide components listed in Table S5 (i.e., Si is as $SiO_2$).

Table S5. Olivine composition in moles and gram-formula weights

| Components | Moles | Formula weights |
|---|---|---|
| $SiO_2$ | 0.6780 | 60.0843 |
| $TiO_2$ | 0.0003 | 79.8658 |
| $Al_2O_3$ | 0.0007 | 101.9613 |
| $Cr_2O_3$ | 0.0001 | 151.9904 |
| FeO* | 0.1384 | 71.8444 |
| MnO | 0.0020 | 70.9374 |
| MgO | 1.2048 | 40.3044 |
| CaO | 0.0038 | 56.0774 |
| $Na_2O$ | 0 | 61.9789 |
| $K_2O$ | 0 | 94.196 |
| $P_2O_5$ | 0 | 141.9445 |
| NiO | 0.0043 | 74.6928 |
| CoO | 0 | 74.932 |

Renormalizing by the total number of the moles (2.0324) gives the olivine composition in mole fractions.

Table S6. Olivine composition expressed as mole fractions

| | |
|---|---|
| $SiO_2$ | 0.3336 |
| $TiO_2$ | 0.0001 |
| $Al_2O_3$ | 0.0003 |
| $Cr_2O_3$ | 0.0000 |
| FeO* | 0.0681 |
| MnO | 0.0010 |
| MgO | 0.5928 |
| CaO | 0.0019 |
| $Na_2O$ | 0 |
| $K_2O$ | 0 |
| $P_2O_5$ | 0 |
| NiO | 0.0021 |
| CoO | 0 |

The following transformation matrix:

| | | | | | | |
|---|---|---|---|---|---|---|
| 1 | –0.5 | –0.5 | –0.5 | –0.5 | –0.5 | –0.5 |
| 0 | 1 | 0 | 0 | 0 | 0 | 0 |
| 0 | 0 | 1 | 0 | 0 | 0 | 0 |
| 0 | 0 | 0 | 1 | 0 | 0 | 0 |
| 0 | 0 | 0 | 0 | 1 | 0 | 0 |
| 0 | 0 | 0 | 0 | 0 | 1 | 0 |
| 0 | 0 | 0 | 0 | 0 | 0 | 1 |

is then multiplied by a vector containing the mole fractions of $SiO_2$, FeO, MnO, MgO, CaO, NiO, and CoO, thereby transforming the olivine composition into moles of end-member olivine components.

Table S7. Olivine composition in moles of end-member components

| | |
|---|---|
| $SiO_2$ | 0.0007 |
| $FeSi_{0.5}O_2$ | 0.0681 |
| $MnSi_{0.5}O_2$, | 0.0010 |
| $MgSi_{0.5}O_2$ | 0.5928 |
| $CaSi_{0.5}O_2$ | 0.0019 |
| $NiSi_{0.5}O_2$ | 0.0021 |
| $CoSi_{0.5}O_2$ | 0 |

The resulting vector is then renormalized by the sum of the olivine-like components, 0.6659 (i.e., excluding $SiO_2$), completing the transformation of an olivine analysis in wt. % to mole fractions of olivine components and $SiO_2$.

Table S8. Olivine composition in mole fractions of end-member components

| | |
|---|---|
| $SiO_2$ | 0.0010 |
| $FeSi_{0.5}O_2$ | 0.1022 |
| $MnSi_{0.5}O_2$, | 0.0015 |
| $MgSi_{0.5}O_2$ | 0.8903 |
| $CaSi_{0.5}O_2$ | 0.0028 |
| $NiSi_{0.5}O_2$ | 0.0032 |
| $CoSi_{0.5}O_2$ | 0 |

Using the values in Tables S6 and S8, the measured $D_{Ni}^{molar}$ (as defined in the main text) is 8.3656

### 1.3 Predicting a partition coefficient

Now that we have transformed our analyses into the necessary molar components (Tables S6 and S8) we have the information we need to predict the partition coefficient. Equation 5 from the main text,

$$-\frac{\Delta_{r(1)}H^{\circ}_{T_{ref},P_{ref}}}{RT}+\frac{\Delta_{r(1)}S^{\circ}_{T_{ref},P_{ref}}}{R}=\ln\left(D^{molar}_{Ni}\right)+\ln\left(\frac{X^{liq}_{MgO}}{X^{ol}_{MgSi_{0.5}O_2}}\right),$$

can be rearranged to yield:

$$D^{molar}_{Ni}=\exp\left[-\frac{\Delta_{r(1)}H^{\circ}_{T_{ref},P_{ref}}}{RT}+\frac{\Delta_{r(1)}S^{\circ}_{T_{ref},P_{ref}}}{R}-\ln\left(\frac{X^{liq}_{MgO}}{X^{ol}_{MgSi_{0.5}O_2}}\right)\right].$$

Based on the fit to the Filter-B dataset, $\frac{-\Delta_{r(1)}H^{\circ}_{T_{ref},P_{ref}}}{R}$ = 4337.9665 and $\frac{\Delta_{r(1)}S^{\circ}_{T_{ref},P_{ref}}}{R}$ = –1.9563, which results in a predicted *molar* partition coefficient, $D^{molar}_{Ni}$, of 9.0630.

### 1.4 Converting $D^{molar}_{Ni}$ to $D^{ol/liq}_{Ni}$

In many applications, it is preferable to work with the traditional weight-based $D^{ol/liq}_{Ni}$. So, in this section, we show how to convert a molar partition coefficient into a weight-based partition coefficient. This conversion is accomplished by multiplying $D^{molar}_{Ni}$ by the ratio of the renormalizing constants used in the olivine transformation and the renormalizing constants used in the liquid transformation. In our example, we renormalized our olivine composition twice (molar sums were 2.0324 and 0.6659) and we renormalized our liquid composition once (molar sum was 2.5449), therefore we need to multiply $D^{molar}_{Ni}$ by 0.5318 [i.e., (2.0324 x0.6659)/2.5449]

to transform the molar partition coefficient to one that is based on weight. The predicted $D_{Ni}^{ol/liq}$ for this example is 4.8195 (the error of the predicted value is ~8%).

## 2. COMPARING FITTED AND TABULATED STANDARD-STATE ENTHALPIES AND ENTROPIES

Here, we compare our fitted values for $-\frac{\Delta_{r(1)}H^{\circ}_{T_{ref},P_{ref}}}{R}$ and $\frac{\Delta_{r(1)}S^{\circ}_{T_{ref},P_{ref}}}{R}$ from equation (5) to those calculated using tabulated thermodynamic data. We used data from Robie *et al.* (1978) whenever possible for these calculations and Barin (1995) when the data was not available in Robie *et al.* (1978) (e.g., the enthalpy of melting of NiO). We took the heat capacity of Ni-olivine from Hirschmann (1991). These data lead to values of $-\frac{\Delta_{r(1)}H^{\circ}_{T_{ref},P_{ref}}}{R}$ and $\frac{\Delta_{r(1)}S^{\circ}_{T_{ref},P_{ref}}}{R}$ of –2171K and –1.6, respectively; these values are roughly comparable in absolute magnitude to the +4338K and –1.96 obtained from fits of Ni partitioning data from the literature (see main text) but $-\frac{\Delta_{r(1)}H^{\circ}_{T_{ref},P_{ref}}}{R}$ is opposite in sign. An alternative technique to determine $-\frac{\Delta_{r(1)}H^{\circ}_{T_{ref},P_{ref}}}{R}$ uses the high-temperature portion (1767 to 1896°C) of the $Ni_2SiO_4$-$Mg_2SiO_4$ phase diagram from Ringwood (1956):we digitized the curves on their Fig. 1 and then used the extracted compositions of coexisting solids and liquids over this temperature interval to calculate partition coefficients, which we then treated in the same manner as our experimental data. Using this method, $-\frac{\Delta_{r(1)}H^{\circ}_{T_{ref},P_{ref}}}{R}$ = –9483K, similar in sign but significantly different in magnitude compared to the value calculated using tabulated thermodynamic data (–2171K). One possible

explanation for the differences in $-\frac{\Delta_{r(1)}H^{\circ}_{T_{ref},P_{ref}}}{R}$ described above, is the apparent dissimilarity between the behavior of Ni in the $Ni_2SiO_4$-$Mg_2SiO_4$ binary and in more complex silicate melts (e.g., Burns & Fyfe 1966).

The preceding analysis indicates that the three different sets of data: experiments in complex systems, experiments along the $Ni_2SiO_4$-$Mg_2SiO_4$ binary, and thermodynamic standard state enthalpies and entropies yield fit parameters that are in poor agreement. For complex silicate melts, activity coefficients are often non-negigible but tend to show relatively small variations over relatively modest changes in composition; in contrast, activity coefficients in simple systems often display much larger variations in response to changes in composition. Ultimately, the overall objective is to fit experimental data in reasonably complex systems with a thermodynamically-inspired function. Although our preferred fit does not reproduce the values calculated from thermodynamic tables, presumably because it includes contributions due to nonideality in the melt, it does quite a good job, as discussed in the main text, of describing our experiments and those from the literature.

## 3. MASS-BALANCE CALCULATIONS

Our mass-balance calculations use the non-linear form of the $\chi^2$ function that includes uncertainties on the oxide values of the bulk composition and each of the phases (e.g., Albarède & Provost 1977). For most phase equilibrium experiments, this is a straightforward exercise. For our experiments and the 1-atm olivine-crucible experiments of Ehlers *et al.* (1992) and Wang & Gaetani (2008), however, this approach must be modified because in these studies the bulk composition for a given experiment is not given by the compositions and mass fractions of the starting olivine and glass. The composition of the liquid evolves during the experiment as it

reacts with the olivine container, but the melt only interacts with a portion of the olivine present within a charge. Thus, at the end of an experiment, the bulk composition actually lies somewhere along a join defined by the starting olivine and glass compositions. Our approach for mass balancing the results of this sort of experimental design is to do a one-dimensional search for the final bulk composition formed by the initial, as weighed glass, and a portion (mass fraction) of the initial, as weighed, olivine that interacted with melt during the experiment, $X^{ol}_{reacted}$. The mass fraction of starting glass is, therefore, $1-X^{ol}_{reacted}$. This bulk composition yields a minimum $\chi^2$ value for the mass balance using the final glass and olivine compositions. The existence of a single minimum is tested by starting at $X^{ol}_{reacted} = 0.99$ and calculating $\chi^2$, then decreasing $X^{ol}_{reacted}$ by 0.025 and again calculating $\chi^2$, and continuing this process till $X^{ol}_{reacted} = 0.015$. Once the minimum is bracketed (multiple minima were not encountered for any experiments), it is refined using inverse parabolic interpolation (e.g., Press *et al.* 1992). Note that one test of internal consistency, which holds true for our experiments, is that $X^{ol}_{reacted}$ cannot exceed the mass fraction of olivine loaded into the capsule.

Since the bulk composition varies with $X^{ol}_{reacted}$, this approach requires a flexible method for calculating one-sigma uncertainties on the bulk. We have calculated fractional errors ($1\sigma$/mean) for large numbers of analyses of different microprobe standards (both glasses and minerals) in the Caltech collection using the same set of analytical conditions that we used for determining the major-element chemistry of our experimental glasses. Standards were chosen so as to cover a broad range of concentrations for the following oxides: $SiO_2$, $TiO_2$, $Al_2O_3$, $Cr_2O_3$, FeO* (all Fe as FeO), MnO, MgO, CaO, $Na_2O$, $K_2O$, and $P_2O_5$. For example, $SiO_2$, FeO*, and MgO concentrations ranged from ~41 to 66, ~6 to 16, and ~0.9 to 49 wt. %, respectively. Our expectation is that fractional errors for a given oxide should be approximately constant for

concentrations above a certain value (generally in the range of 1 to 2 wt. %, although this will vary with the oxide). Below this concentration range, fractional errors increase rapidly, eventually exceeding a value of one; a concentration that yields a fractional error of one is assumed to be close to the detection limit. For the ranges of silica and iron concentrations reported above, fractional errors were, not surprisingly, uncorrelated with concentration and we calculated the following mean value: 0.003829. Thus, for a given bulk $SiO_2$ value, the corresponding standard deviation would be: wt. % $SiO_2 \times 0.003829$. For MgO, fractional errors are not constant over the concentration range of 0.9 to 49 wt. % and have been fit using the following power law expression: $\boldsymbol{a} + \boldsymbol{b} \times (\text{wt. \% MgO})^{\boldsymbol{c}}$, (where $\boldsymbol{a}$, $\boldsymbol{b}$, and $\boldsymbol{c}$ are the fit parameters). The remaining oxides also spanned a sufficient compositional range so as to require non-constant fractional errors, which were fit using either: $\boldsymbol{a} \times (\text{wt. \% of oxide } i)^{\boldsymbol{b}}$ or $\boldsymbol{a} + \boldsymbol{b} \times (\text{wt. \% of oxide } i)^{\boldsymbol{c}}$. Fig. S2 shows fits for MgO and $K_2O$.

Note that the list of oxides considered in the previous paragraph does not include NiO. We treat bulk NiO as a free parameter in our mass balance calculations because this element is easily lost from our high-pressure experiments if melt comes into contact with the graphite inner capsule. To ensure a good mass balance fit for Ni (and thus an accurate estimate of Ni loss or gain), we fix the fractional error for NiO in all phases and in the bulk at 0.001. The difference between $NiO^{bulk}$ required for mass balance and the NiO concentration calculated using the optimal value of $X^{ol}_{reacted}$ and the NiO contents of the starting olivine and glass is a metric for the extent to which NiO has been conserved in a given experiment. For 1-atm olivine-capsule experiments, we also allowed bulk $Na_2O$ to vary in the mass balance calculations because of the well-known volatility of sodium (e.g., Corrigan & Gibb 1979; Kilinc *et al.* 1983; Yamanaka *et al.* 1996). If the concentration of bulk NiO and/or $Na_2O$ (in 1-atm runs) changes, then the

remaining oxide concentrations in the bulk change inversely by a proportional amount (i.e., the bulk oxide sum remains fixed at 100%). For each experiment, the minimum $\chi^2$ value along with the number of degrees of freedom is used to calculate a *Q* value, a statistical measure of goodness-of-fit (the degrees of freedom are decreased by the number of oxides in the bulk that are allowed to vary).

Several further points concerning our mass-balance approach for olivine-capsule experiments are worth discussing: the method is based on the assumption that dissolution/reprecipitation of olivine is the dominant process that causes the liquid to evolve in composition. If the liquid composition at the end of an experiment is largely controlled by differing rates of diffusion of components into and out of the olivine capsule, we would expect that this mass balance approach would not yield successful solutions. The fact that we do generate successful solutions suggests that dissolution/reprecipitation is probably the dominant mechanism generating a change in liquid composition. Finally, our approach fails if the final liquid and olivine compositions are too similar to those of the starting olivine and glass—i.e., little dissolution/reprecipitation has occurred during the experiment. In this case, the starting olivine and glass pair and the final olivine and glass pair are, within error, collinear.

For experiments from the literature run on wire loops or in precious metal capsules ± graphite, the bulk composition is, in principle, fixed, except for elements soluble in the container material, and the mass-balance approach is more straight-forward, although as stated above the inclusion of errors on the phase compositions makes the $\chi^2$ equation non-linear. However, only a subset of studies in our database report analytical uncertainties on the average phase compositions and very few provide estimates of the uncertainties on their bulk compositions. Thus, a consistent approach is required for estimating these uncertainties. The experimental

olivine-liquid Ni partitioning studies in our literature database span nearly four decades and much of the data was collected using earlier generations of microprobes. So we used the large body of average experimental glass compositions and uncertainties published by the MIT group (all collected on a JEOL 733 microprobe) to calculate fractional errors for the following oxides: $SiO_2$, $TiO_2$, $Al_2O_3$, $Cr_2O_3$, FeO* (all Fe as FeO), MnO, MgO, CaO, $Na_2O$, $K_2O$, and $P_2O_5$. As with our data obtained on a JEOL 8200, fractional errors for $SiO_2$ are independent of concentration in the range 35–71 wt. % and have a mean value of 0.006480. For the remaining oxides, power law fits adequately describe the variation of fractional error with concentration. Again, the fractional error for NiO in all phases and in the bulk was set to 0.001 and bulk NiO was a free parameter in the mass balance calculations. For the 1-atm wire loop and Mo crucible experiments, bulk FeO*, $Na_2O$, and $K_2O$ concentrations were also allowed to vary: the alkalis for reasons of volatility and FeO* because, even with pre-saturation of the sample container, a silicate charge can nevertheless gain or lose Fe. Further, for the experiments of Synder & Carmichael (1992) done on Fe-wire loops, the silicate charges gained substantial amounts of iron (note that this does not necessarily mean that these experiments have not closely approached equilibrium). For the high-pressure experiments in the database, only bulk Ni was allowed to vary. Finally, a goodness-of-fit parameter *Q* was calculated for each mass balance calculation using the $\chi^2$ value and the number of degrees of freedom. A manuscript describing the olivine-capsule mass-balance program is in preparation.

## 4. CONSTRUCTING THE FILTER-B DATASET

The only filter used in constructing our Filter-A dataset is the constraint that the oxide sums for both olivine and liquid lie in the range from 98.5 to 101.5. Note that Hart & Davis (1978) did not

give complete olivine analyses; for these experiments, we calculated $SiO_2$ in the olivine based on an ideal $MSi_{0.5}O_2$ stoichiometry. Our fit to this loosely-filtered dataset produces relatively large residuals (e.g., using equation (5) the mean percent error on $D_{Ni}^{ol/liq}$ is ~14%). As discussed in the main text, a flux of Ni out of the silicate portion of the charge and into the container or wire-loop can lead to anomalous $D_{Ni}^{ol/liq}$ values. Thus, the following question arises: Is the scatter in the fits to our models a result of the shortcomings of our models, the lack of equilibrium in some experiments, or poor data quality? To partially address this inherently difficult question, we developed a more restrictive Filter-B dataset. Ideally, such a dataset would contain only well-analyzed, equilibrium experiments but achieving this goal proved elusive. We began with all of the experiments in the Filter-A dataset and mass balanced each experiment; those experiments that yielded successful solutions at the 95% confidence level were included in the provisional Filter-B dataset. Recall that in order to evaluate the extent to which bulk Ni changed during a given experiment, the starting concentration of NiO was treated as a variable in our mass balance calculations, and thus a successful mass balance solution does not necessarily mean that nickel was conserved. A number of experimental studies (experiments from Leeman 1974, run above 1300°C and >144 hrs; Arndt 1977; Hart & Davis 1978; experiments from Takahashi 1978, run above 1320°C and >15 hrs; Campbell *et al.* 1979; Nabelek 1980; Drake & Holloway 1981; Seifert *et al.* 1988; Kinzler *et al.* 1990; Snyder & Carmichael 1992; Mysen 2006; Mysen 2007) explicitly demonstrated (e.g., via time-series experiments) that $D_{Ni}^{ol/liq}$ had reached equilibrium despite relatively large changes in bulk Ni. For example, Run 14 from Hart & Davis (1978) passes our mass balance test even though our calculations suggest that it lost 58% of the initial NiO in the bulk composition. Despite large amounts of Ni-loss, Hart & Davis (1978) demonstrated that their run times were sufficient for Ni to equilibrate between the olivine, liquid,

and Pt wire loop or Pt capsule, and thus all Hart & Davis experiments that satisfy mass balance (irrespective of Ni-loss) were included in the provisional Filter-B dataset. We took a different approach for experiments lacking any explicit demonstration of equilibrium. We computed NiO loss for all such experiments and then steadily expanded the acceptance limit for percent change in bulk NiO, thereby allowing more experiments into the provisional Filter-B dataset, and then observed how the residual sum of squares increases for model fits to equation 5. We found that the residual sum of squares increased rapidly if experiments that had lost or gained more than 70% of their initial NiO were included in the provisional Filter-B dataset. We interpreted this result to indicate that a significant fraction of these experiments did not achieve equilibrium (i.e., some of these experiments may have achieved equilibrium but others had not). Thus, the final Filter-B dataset includes only those experiments for which the bulk Ni changed by less than 65% relative, all other oxides satisfy mass balance, and oxide sums are between 98.5 and 101.5 wt%.

## 5. FITTING $D_{Ni}^{ol/liq}$ USING A REGULAR SOLUTION MODEL

The fits described in the main text assume that the melt and olivine behave as ideal solutions. This is a reasonable first-order assumption for olivine at high temperatures (e.g., Nafziger & Muan 1967; Campbell & Roeder 1968; Seifert & O'Neill 1987; Wiser & Wood 1991); for liquids, however, this assumption is much less likely to hold, particularly over the large compositional range represented by the Filter-A and -B databases.

In this section, we depart from treating the melt as an ideal solution by adding simplified regular-solution-like terms to our model in an effort to account for the interactions among liquid $SiO_2$, MgO, and NiO and the effect they may have on the observed variations in $D_{Ni}^{ol/liq}$. It is important to note that the existing experimental database is not well posed for a full regular-

solution treatment (e.g., Kinzler *et al.* 1990). Although not thermodynamically rigorous, the approach we have chosen nominally accounts simultaneously for the effects of MgO and $SiO_2$ in the melt, and allows us to evaluate whether the small, but non-negligible, variations of these components in the liquids in our experiments contribute significantly to the observed variations in $D_{Ni}^{ol/liq}$.

Using equation 10 from Ghiorso *et al.* (1983), we formulated expressions for the activity coefficients of liquid NiO, MgO, and $Si_{0.5}O$ in the $Si_{0.5}O$-NiO-MgO ternary:

$$RT\ln\gamma_{MgO}^{liq} = W_{Ni-Mg}X_{NiO}^{liq}\left(1-X_{MgO}^{liq}\right)+W_{Mg-Si}X_{Si_{0.5}O}^{liq}\left(1-X_{MgO}^{liq}\right)-W_{Ni-Si}X_{NiO}^{liq}X_{Si_{0.5}O}^{liq} \quad \text{(S1)}$$

$$RT\ln\gamma_{NiO}^{liq} = W_{Ni-Mg}X_{MgO}^{liq}\left(1-X_{NiO}^{liq}\right)+W_{Ni-Si}X_{Si_{0.5}O}^{liq}\left(1-X_{NiO}^{liq}\right)-W_{Mg-Si}X_{MgO}^{liq}X_{Si_{0.5}O}^{liq} \quad \text{(S2)}$$

$$RT\ln\gamma_{Si_{0.5}O}^{liq} = W_{Ni-Si}X_{NiO}^{liq}\left(1-X_{Si_{0.5}O}^{liq}\right)+W_{Mg-Si}X_{MgO}^{liq}\left(1-X_{Si_{0.5}O}^{liq}\right)-W_{Mg-Ni}X_{MgO}^{liq}X_{NiO}^{liq} \quad \text{(S3).}$$

We chose the $Si_{0.5}O$-NiO-MgO ternary as a basis because both Si (e.g., Li & Ripley 2010) and Mg (e.g., Hart & Davis 1978) are thought to influence Ni partitioning. Combining equations (S1) and (S2) with the exchange reaction (equation 4, from main text) makes the exchange reaction an explicit function of the Mg, Ni, *and Si* contents of the liquid:

$$-\frac{\Delta_{r(1)}H^{\circ}_{T_{ref},P_{ref}}}{RT}+\frac{\Delta_{r(1)}S^{\circ}_{T_{ref},P_{ref}}}{R}-\frac{W_{Ni-Mg}\left(X_{NiO}^{liq}-X_{MgO}^{liq}\right)}{RT}-\frac{\left(W_{Mg-Si}-W_{Si-Ni}\right)X_{Si_{0.5}O}^{liq}}{RT}=\ln\left(D_{Ni}^{molar}\right)..$$
$$+\ln\left(\frac{X_{MgO}^{liq}}{X_{MgSi_{0.5}O_2}^{ol}}\right)+\frac{\int_{T_{ref}}^{T}\Delta_{r(1)}C_p^{\circ}dT}{RT}-\frac{\int_{T_{ref}}^{T}\left(\Delta_{r(1)}C_p^{\circ}/T\right)dT}{R}+\frac{\int_{P_{ref}}^{P}\Delta_{r(1)}VdP}{RT} \quad \text{(S4).}$$

Similarly, substituting expressions for $\gamma_{NiO}^{liq}$ and $\gamma_{Si_{0.5}O}^{liq}$ (S2) and (S3) into the formation reaction, (equation (7), from the main text), gives

$$-\frac{\Delta_{r(6)}H^{\circ}_{T_{ref},P_{ref}}}{RT}+\frac{\Delta_{r(6)}S^{\circ}_{T_{ref},P_{ref}}}{R}=\ln\left(D^{molar}_{Ni}\right)+\ln\left(\frac{1}{X^{liq}_{Si_{0.5}O}}\right)+\frac{\int_{P_{ref}}^{P}\Delta_{r(6)}VdP}{RT}+\frac{\int_{T_{ref}}^{T}\Delta_{r(6)}C^{\circ}_{p}dT}{RT}-\frac{\int_{T_{ref}}^{T}\left(\frac{\Delta_{r(6)}C^{\circ}_{p}}{T}\right)dT}{R}\ldots$$
$$+\frac{W_{Ni-Mg}X^{liq}_{MgO}\left(2X^{liq}_{NiO}-1\right)}{RT}+\frac{W_{Si-Mg}X^{liq}_{MgO}\left(2X^{liq}_{Si_{0.5}O}-1\right)}{RT}+\frac{W_{Ni-Si}\left(X^{liq}_{NiO}\left(2X^{liq}_{Si_{0.5}O}-1\right)-X^{liq}_{Si_{0.5}O}\right)}{RT}$$

(S5).

In order to be self-consistent, we used a non-linear least squares algorithm (Levenberg-Marquardt implemented in MATLAB) to simultaneously solve for the standard state enthalpy and entropy of both the exchange (S4) and formation reactions (S5), along with the three common interaction parameters listed above. By fitting equations (S4) and (S5) simultaneously, we ensured that the fitted standard-state and interaction parameters for both reactions were self-consistent e.g.,

$\Delta_{r(6)}H^{\circ}_{T_{ref},P_{ref}}=\Delta_{r(1)}H^{\circ}_{T_{ref},P_{ref}}+H^{\circ}_{T_{ref},P_{ref}}(X^{ol}_{MgSi_{0.5}O_2})-H^{\circ}_{T_{ref},P_{ref}}(X^{liq}_{MgO})-H^{\circ}_{T_{ref},P_{ref}}(X^{liq}_{NiO})$ and ($W_{Mg\text{-}Si}-W_{Si\text{-}Ni}$)(S4) = $W_{Mg\text{-}Si}$(S4) – $W_{Si\text{-}Ni}$(S5), where (S4) and (S5) refer to the source equations. Fitted values for both the Filter-A and Filter-B datasets are listed in Table S2. For the exchange reaction and the Filter-B dataset, adding three new fit parameters does not significantly change the quality of the fit (the mean percent error increases from 12.0 to 12.3%). The quality of the fit to the formation reaction using the Filter-B dataset improves markedly; the mean percent error on $D^{ol/liq}_{Ni}$ decreases from 15.6 to 10.9%. These results illustrate why working with an exchange reaction in complex systems is generally preferable to using a formation reaction if the objective is to minimize the effects of melt non-ideality when calculating model partition coefficients.

Although the quality of the fit to the formation reaction improves by adding non-ideal terms, our pseudoternary liquid model is clearly too simplistic; the residuals of our non-ideal

models are correlated with concentrations of liquid components and higher order combinations of these concentrations. We did not pursue a more complicated model because, even if one could evaluate the constants for all interaction parameters for a 7-12 component liquid, it is quite unlikely that a regular solution can be applied over the broad composition range found in the Filter-A and Filter-B datasets. Properly resolving the full compositional dependence of $D_{Ni}^{ol/liq}$ will require a substantially larger experimental database and one that is better posed to extract specific interaction parameters. Nevertheless, our experiments provide an important step in characterizing the factors that influence $D_{Ni}^{ol/liq}$ by better distinguishing between contributions due to variations in phase compositions and those due to variations in temperature and pressure. Even our simplistic treatments via equations (S4) and (S5) makes the exchange reaction an explicit function of the silica content of the liquid and it makes the formation reaction an explicit function of the MgO content of the liquid. This is important as it allows us to test whether or not the variations in liquid composition observed in our experiments could plausibly lead to the observed variations in $D_{Ni}^{ol/liq}$ and therefore the extent to which we have succeeded in isolating the role of temperature from that of phase composition.

To perform this test, we compare the measured $D_{Ni}^{ol/liq}$ from our experiments to the predicted partition coefficient for an olivine-liquid pair in which phase compositions are held constant but pressure and temperature are increased. Figure S3 shows the predicted partition coefficient for a constant composition olivine-liquid pair using the fits to equations (S4) and (S5) and the Filter-A and Filter-B databases. Also shown on Fig. S3 is the measured $D_{Ni}^{ol/liq}$ from each of our experiments. Our experiments, which do vary slightly in composition, are in good agreement with the prediction for a constant composition olivine-liquid pair, suggesting that the effect of temperature and pressure, rather than that of composition, is the dominant driver of the

observed variation in $D_{Ni}^{ol/liq}$. Additionally, we can obtain a sense for the magnitude of the compositional effect by comparing, at the same temperature and pressure, the predicted partition coefficient for liquids with different compositions (recall that our high-pressure experiments crystallized pyroxene and thus produced a liquid with lower $SiO_2$ and higher incompatible element concentrations than our experiments that did not undergo pyroxene crystallization). To perform this calculation we use the coexisting olivine and liquid compositions from two experiments (Run 25, a "normal" experiment; and Run 33R, an experiment whose liquid contained lower $SiO_2$ due to pyroxene crystallization), although we could have also used synthetic olivine and liquid compositions. Using the phase compositions, temperature, and pressure from Run 33R (45.40 wt. % $SiO_2$ and 16.31 wt. MgO in the glass, 3.0 GPa and 1550°C), model S4 (Filter-B dataset) predicts a $D_{Ni}^{ol/liq}$ of 4.39; this is close to the prediction using the composition of run 25 (48.26 and 17.17 wt. % $SiO_2$ and MgO in the glass, respectively) taken to 3.0 GPa and 1550°C, for which the same model predicts a $D_{Ni}^{ol/liq}$ of 4.17. This small (0.22 or ~5%) difference in $D_{Ni}^{ol/liq}$ is well within our typical errors, and as stated above, these calculations suggest that the small changes in liquid composition observed in our experiments cannot account for the ~24 % drop in $D_{Ni}^{ol/liq}$ from ~5.0 at 1-atm to ~3.8 at 3.0 GPa and 1550°C.

## 6. COMMENTS ON THE JONES-BEATTIE MODEL

The explicitly temperature-independent partitioning models of Jones (1984) and Beattie *et al.* (1991) are widely used in geochemical modeling (e.g., Sobolev *et al.* 2005; Herzberg 2011) due to the simple functional form, $D_{Ni}^{cation} = A \times D_{Mg}^{cation} + B$ (where *A* and *B* are fit parameters), and the expressions' ability to recover experimentally produced $D_{Ni}^{ol/liq}$s from a wide range of olivine and glass compositions (e.g., Filiberto *et al.* 2009). For the Filter-A and -B datasets, the apparent

correlation between $D_{Ni}^{molar}$ and $D_{Mg}^{molar}$ (where $D_{Mg}^{molar} = \frac{X_{MgSi_{0.5}O_2}^{ol}}{X_{MgO}^{liq}}$) is better than the correlation between $\ln\left(D_{Ni}^{molar}\right) + \ln\left(\frac{X_{MgO}^{liq}}{X_{MgSi_{0.5}O_2}^{ol}}\right)$ and $1/T$. Thus, it is a natural starting point for an empirical partitioning expression, but such an expression appears to conflict with our experimental data, which clearly demonstrates that at constant $D_{Mg}^{ol/liq}$, $D_{Ni}^{ol/liq}$ varies systematically from 1400 to 1550°C, suggesting that $D_{Ni}^{ol/liq}$ is, in fact, temperature dependent. Here, we show how the correlation between $D_{Mg}^{molar}$ and temperature can lead to an expression for $D_{Ni}^{ol/liq}$ that spuriously appears to be independent of temperature.

Rearranging equation (5) from the main text and substituting in the above definition of $D_{Mg}^{molar}$ we are left with an expression relating $D_{Ni}^{molar}$ and $D_{Mg}^{molar}$:

$$D_{Ni}^{molar} = \left[ e^{-\frac{\Delta_{r(1)}H^{\circ}_{T_{ref},P_{ref}}}{RT} + \frac{\Delta_{r(1)}S^{\circ}_{T_{ref},P_{ref}}}{R}} \right] D_{Mg}^{molar} \qquad \text{(S6).}$$

This equation is just a rearrangement of equation (5) and, therefore, contains no additional assumptions. The terms $\Delta_{r(1)}C_p^{\circ}$ and $\Delta_{r(1)}V$ and the activity coefficient term in equation (4) are assumed to be zero (or, if the phases are Henrian, the $\frac{\Delta_{r(1)}S^{\circ}_{T_{ref},P_{ref}}}{R}$ term would be a combination of the true $\frac{\Delta_{r(1)}S^{\circ}_{T_{ref},P_{ref}}}{R}$ and a term involving the ratio of the activity coefficients). The functional form of equation (S6) suggests that, as $D_{Mg}^{molar}$ approaches zero, so should $D_{Ni}^{molar}$; additionally, if $\Delta_{r(1)}H^{\circ}_{T_{ref},P_{ref}}$ is zero (i.e., the equilibrium constant of the exchange reaction is temperature independent), equation (S6) predicts a linear relationship between $D_{Ni}^{molar}$ and $D_{Mg}^{molar}$ with a y intercept of zero. Beattie *et al.* (1991) showed that, for elements other than Ni, this is often true (e.g., plots of $D_{Mn}^{cation}$ and $D_{Fe}^{cation}$ vs. $D_{Mg}^{cation}$ are linear and have y intercepts of zero; see their Fig. 4), whereas the correlation between $D_{Ni}^{cation}$ vs. $D_{Mg}^{cation}$ is roughly linear but has a y intercept of approximately –3.5.

As mentioned in the Introduction and illustrated in Fig. S4a for our Filter-A compilation of Ni-partitioning experiments, $D_{Mg}^{molar}$ and temperature are correlated. Figure S4a shows that the natural log of $D_{Mg}^{molar}$ and inverse temperature (in Kelvin) is also well described by either a linear or a 3$^{rd}$ –order-polynomial (cubic) fit. Replacing the *1/T* term in equation (S6) using the linear fit for 1/*T* from Figure S4a, leads to

$$D_{Ni}^{molar} = \left[ e^{-\frac{\Delta_{r(1)} H^{\circ}_{T_{ref},P_{ref}}}{R}\left(\alpha \times \ln(D_{Mg}^{molar}) + \beta\right) + \frac{\Delta_{r(1)} S^{\circ}_{T_{ref},P_{ref}}}{R}} \right] D_{Mg}^{molar}, \qquad \text{(S7)}$$

where α and β are the slope and, intercept from the linear fit shown in Fig. S4a (although not shown, an analogous expression can be derived using the cubic fit in Fig. S4a).

Figure S4b shows the predicted relationship between $D_{Ni}^{molar}$ and $D_{Mg}^{molar}$ obtained by combining $-\frac{\Delta_{r(1)} H^{\circ}_{T_{ref},P_{ref}}}{R}$ and $\frac{\Delta_{r(1)} S^{\circ}_{T_{ref},P_{ref}}}{R}$ from the fit to equation (5) using the Filter-A dataset (see Discussion and Table 4 from the main text), the relationships between $D_{Mg}^{molar}$ and temperature from Fig. S4a, and the measured $D_{Ni}^{molar}$ and $D_{Mg}^{molar}$ of experiments in the Filter-A dataset. This figure illustrates that using our standard state enthalpies and entropies of reaction (1) in conjunction with the correlation between $D_{Mg}^{molar}$ and temperature of the experimental database does a good job of predicting the observed $D_{Ni}^{molar}$ [note that Jones (2010) predicts a different relationship between $D_{Ni}^{molar}$ and $D_{Mg}^{molar}$ at and below a $D_{Mg}^{molar}$ of ~2 and in light of the shortage of experimental data in this region extreme care should be used when extrapolating our model to such low values of $D_{Mg}^{molar}$ ]. There is no reason to expect, however, that $D_{Mg}^{molar}$ and temperature will vary the same way in nature as it does for the experimental database. Therefore, the Jones-Beattie functional form may be ill suited to natural applications, or experiments such as ours, where the variation between $D_{Mg}^{molar}$ and temperature is different from that of the experimental database.

**REFERENCES FOR SECTIONS 1-6**


Albarède, F. & Provost, A. (1977). Petrological and geochemical mass-balance equations: an algorithm for least-square fitting and general error analysis. *Computers and Geosciences* **3**, 309-326.

Arndt, N. T. (1977). Partitioning of nickel between olivine and ultrabasic and basic komatiite liquids. *Year Book - Carnegie Institution of Washington* **76**, 553-557.

Baker, M. B., Alves, S. & Stolper, E. M. (1996). Petrography and petrology of the Hawaii Scientific Drilling Project lavas: Inferences from olivine phenocryst abundances and compositions. *Journal of Geophysical Research* **101**, 11715-11727.

Barin, I. (1995). *Thermochemical data of pure substances*. VCH: New York.

Beattie, P., Ford, C. & Russell, D. (1991). Partition coefficients for olivine-melt and orthopyroxene-melt systems. *Contributions to Mineralogy and Petrology* **109**, 212-224.

Burns, R. G. & Fyfe, W. S. (1966). Behaviour of nickel during magmatic crystallization. *Nature* **210**, 1147-1148.

Campbell, F. E. & Roeder, P. (1968). The stability of olivine and pyroxene in the Ni-Mg-Si-O system. *American Mineralogist* **53**, 257-268.

Campbell, I. H., Naldrett, A. J. & Roeder, P. L. (1979). Nickel activity in silicate liquids: some preliminary results. *The Canadian Mineralogist* **17**, 495-505.

Clague, D. A., Weber, W. S. & Dixon, J. E. (1991). Picritic glasses from Hawaii. *Nature* **353**, 553-556.

Corrigan, G. & Gibb, F. G. F. (1979). Loss of Fe and Na from a basaltic melt during experiments Using the wire-loop method. *Mineralogical Magazine* **43**, 121-126.

Drake, M. J. & Holloway, J. R. (1981). Partitioning of Ni between olivine and silicate melt: the 'Henry's Law problem' reexamined. *Geochimica et Cosmochimica Acta* **45**, 431-437.

Ehlers, K., Grove, T. L., Sisson, T. W., Recca, S. I. & Zervas, D. A. (1992). The effect of oxygen fugacity on the partitioning of nickel and cobalt between olivine, silicate melt, and metal. *Geochimica et Cosmochimica Acta* **56**, 3733-3743.

Filiberto, J., Jackson, C., Le, L. & Treiman, A. H. (2009). Partitioning of Ni between olivine and an iron-rich basalt: Experiments, partition models, and planetary implications. *American Mineralogist* **94**, 256-261.

Ghiorso, M. S., Carmichael, I. S. E., Rivers, M. L. & Sack, R. O. (1983). The Gibbs free-energy of mixing of natural silicate liquids—an expanded regular solution approximation for the calculation of magmatic intensive variables. *Contributions to Mineralogy and Petrology* **84**, 107-145.

Hart, S. R. & Davis, K. E. (1978). Nickel partitioning between olivine and silicate melt. *Earth and Planetary Science Letters* **40**, 203-219.

Herzberg, C. (2006). Petrology and thermal structure of the Hawaiian plume from Mauna Kea volcano. *Nature* **444**, 605-609.

Herzberg, C. (2011). Identification of source lithology in the Hawaiian and Canary islands: Implications for origins. *Journal of Petrology* **52**, 113-146.

Herzberg, C. & O'Hara, M. J. (2002). Plume-associated ultramafic magmas of Phanerozoic age. *Journal of Petrology* **43**, 1857-1883.

Hirschmann, M. (1991). Thermodynamics of multicomponent olivines and the solution properties of $(Ni,Mg,Fe)_2SiO_4$ and $(Ca,Mg,Fe)_2SiO_4$ olivines. *American Mineralogist* **76**, 1232-1248.

Jones, J. H. (1984). Temperature- and pressure-independent correlations of olivine/liquid partition coefficients and their application to trace-element partitioning. *Contributions to Mineralogy and Petrology* **88**, 126-132.

Jones, J. H. (2010). Variations on a theme by Longhi: I. An analysis of the thermodynamic underpinning of Fe, Mn, and Ni partitioning into olivine. *41st Lunar and Planetary Science Conference*, Abstract 1338.

Kilinc, A., Carmichael, I. S. E., Rivers, M. L. & Sack, R. O. (1983). The ferric-ferrous ratio of natural silicate liquids equilibrated in air. *Contributions to Mineralogy and Petrology* **83**, 136-140.

Kinzler, R. J., Grove, T. L. & Recca, S. I. (1990). An experimental study on the effect of temperature and melt composition on the partitioning of nickel between olivine and silicate melt. *Geochimica et Cosmochimica Acta* **54**, 1255-1265.

Leeman, W. P. (1974). Part I, Petrology of basaltic lavas from the Snake River Plain, Idaho; and Part II, Experimental determination of partitioning of divalent cations between olivine and basaltic liquid. Doctoral dissertation thesis, University of Oregon.

Li, C. & Ripley, E. M. (2010). The relative effects of composition and temperature on olivine-liquid Ni partitioning: Statistical deconvolution and implications for petrologic modeling. *Chemical Geology* **275**, 99-104.

Matzen, A. K., Baker, M. B., Beckett, J. R. & Stolper, E. M. (2011). Fe–Mg partitioning between olivine and high-magnesian melts and the nature of Hawaiian parental liquids. *Journal of Petrology* **52**, 1243-1263.

Mysen, B. (2007). Partitioning of calcium, magnesium, and transition metals between olivine and melt governed by the structure of the silicate melt at ambient pressure. *American Mineralogist* **92**, 844-862.

Mysen, B. O. (2006). Redox equilibria of iron and silicate melt structure: Implications for olivine/melt element partitioning. *Geochimica et Cosmochimica Acta* **70**, 3121-3138.

Nabelek, P. I. (1980). Nickel partitioning between olivine and liquid in natural basalts: Henry's law behavior. *Earth and Planetary Science Letters* **48**, 293-302.

Nafziger, R. H. & Muan, A. (1967). Equilibrium phase compositions and thermodynamic properties of olivines and pyroxenes in system MgO-"FeO"-$SiO_2$. *American Mineralogist* **52**, 1364-1385.

Press, W. H., Teukolsky, S. A., Vetterling, W. T. & Flannery, B. P. (1992). *Numerical Recipes*. Cambridge University Press: Cambridge.

Ringwood, A. E. (1956). Melting relationships of Ni-Mg olivines and some geochemical implications. *Geochimica et Cosmochimica Acta* **10**, 297-303.

Robie, R. A., Hemingway, B. S. & Fisher, J. R. (1978). Thermodynamic properties of minerals and related substances at 298.15 K and 1 bar ($10^5$ Pascals) pressure and at higher temperatures. *U.S. Geological Survey Bulletin* **1452**.

Seifert, S. & O'Neill, H. St. C. (1987). Experimental determination of activity-composition relations in $Ni_2SiO_4$-$Mg_2SiO_4$ and $Co_2SiO_4$-$Mg_2SiO_4$ olivine solid solutions at 1200 K and 0.1 MPa and 1573 K and 0.5 GPa. *Geochimica et Cosmochimica Acta* **51**, 97-104.

Seifert, S., O'Neill, H. St. C. & Brey, G. (1988). The partitioning of Fe, Ni and Co between olivine, metal, and basaltic liquid: An experimental and thermodynamic investigation, with application to the composition of the lunar core. *Geochimica et Cosmochimica Acta* **52**, 603-616.

Snyder, D. A. & Carmichael, I. S. E. (1992). Olivine-liquid equilibria and the chemical activities of FeO, NiO, $Fe_2O_3$, and MgO in natural basic melts. *Geochimica et Cosmochimica Acta* **56**, 303-318.

Sobolev, A. V., Hofmann, A. W., Sobolev, S. V. & Nikogosian, I. K. (2005). An olivine-free mantle source of Hawaiian shield basalts. *Nature* **434**, 590-597.

Stolper, E., Sherman, S., Garcia, M., Baker, M. & Seaman, C. (2004). Glass in the submarine section of the HSDP2 drill core, Hilo, Hawaii. *Geochemistry Geophysics Geosystems* **5**, Q07G15, doi:10.1029/2003GC000553.

Takahashi, E. (1978). Partitioning of $Ni^{2+}$, $Co^{2+}$, $Fe^{2+}$, $Mn^{2+}$ and $Mg^{2+}$ between olivine and silicate melts: compositional dependence of partition coefficient. *Geochimica et Cosmochimica Acta* **42**, 1829-1844.

Wang, Z. & Gaetani, G. A. (2008). Partitioning of Ni between olivine and siliceous eclogite partial melt: experimental constraints on the mantle source of Hawaiian basalts. *Contributions to Mineralogy and Petrology* **156**, 661-678.

Wiser, N. M. & Wood, B. J. (1991). Experimental determination of activities in Fe-Mg olivine at 1400 K. *Contributions to Mineralogy and Petrology* **108**, 146-153.

Wright, T. L. (1984). Origin of Hawaiian tholeiite: a metasomatic model. *Journal of Geophysical Research* **89**, 3233-3252.

Yamanaka, A., Tsuchiyama, A., Tachibana, S. & Kawamura, K. (1996). Measurements of evaporation rates of sodium and potassium from silicate melts. *Papers Presented to the 21$^{st}$ Symposium on Antarctic Meteorites*, 210-212.

## 7. EXPERIMENTAL DATABASE REFERENCES

In addition to the data from this work we considered experiments from the following sources. See the main text and Section 4 of this Supplement for the criterion by which subsets of this dataset were selected.


Agee, C. B. & Walker, D. (1990). Aluminum partitioning between olivine and ultrabasic silicate liquid to 6 GPa. *Contributions to Mineralogy and Petrology* **105**, 243-254.

Arndt, N. T. (1977). Partitioning of nickel between olivine and ultrabasic and basic komatiite liquids. *Year Book - Carnegie Institution of Washington*, 553-557.

Bickle, M. J., Ford, C. E. & Nisbet, E. G. (1977). Petrogenesis of peridotitic komatiites: Evidence from high-pressure melting experiments. *Earth and Planetary Science Letters* **37**, 97-106.

Brenan, J. M., McDonough, W. F. & Ash, R. (2005). An experimental study of the solubility and partitioning of iridium, osmium and gold between olivine and silicate melt. *Earth and Planetary Science Letters* **237**, 855-872.

Campbell, I. H., Naldrett, A. J. & Roeder, P. L. (1979). Nickel activity in silicate liquids: some preliminary results. *The Canadian Mineralogist* **17**, 495-505.

Drake, M. J. & Holloway, J. R. (1981). Partitioning of Ni between olivine and silicate melt: the 'Henry's Law problem' reexamined. *Geochimica et Cosmochimica Acta* **45**, 431-437.

Ehlers, K., Grove, T. L., Sisson, T. W., Recca, S. I. & Zervas, D. A. (1992). The effect of oxygen fugacity on the partitioning of nickel and cobalt between olivine, silicate melt, and metal. *Geochimica et Cosmochimica Acta* **56**, 3733-3743.

Filiberto, J., Jackson, C., Le, L. & Treiman, A. H. (2009). Partitioning of Ni between olivine and an iron-rich basalt: Experiments, partition models, and planetary implications. *American Mineralogist* **94**, 256-261.

Hart, S. R. & Davis, K. E. (1978). Nickel partitioning between olivine and silicate melt. *Earth and Planetary Science Letters* **40**, 203-219.

Herd, C. D. K., Dwarzski, R. E. & Shearer, C. K. (2009). The behavior of Co and Ni in olivine in planetary basalts: An experimental investigation. *American Mineralogist* **94**, 244-255.

Herzberg, C. & Zhang, J. (1996). Melting experiments on anhydrous peridotite KLB-1: Compositions of magmas in the upper mantle and transition zone. *Journal of Geophysical Research* **101**, 8271-8295.

Jurewicz, A. J. G., Mittlefehldt, D. W. & Jones, J. H. (1993). Experimental partial melting of the Allende (CV) and Murchison (CM) chondrites and the origin of asteroidal basalts. *Geochimica et Cosmochimica Acta* **57**, 2123-2139.

Kinzler, R. J., Grove, T. L. & Recca, S. I. (1990). An experimental study on the effect of temperature and melt composition on the partitioning of nickel between olivine and silicate melt. *Geochimica et Cosmochimica Acta* **54**, 1255-1265.

Le Roux, V., Dasgupta, R. & Lee, C. T. A. (2011). Mineralogical heterogeneities in the Earth's mantle: Constraints from Mn, Co, Ni and Zn partitioning during partial melting. *Earth and Planetary Science Letters* **307**, 395-408.

Leeman, W. P. (1974). Part I, Petrology of basaltic lavas from the Snake River Plain, Idaho; and Part II, Experimental determination of partitioning of divalent cations between olivine and basaltic liquid. Doctoral dissertation thesis, University of Oregon.

Longhi, J., Durand, S. R. & Walker, D. (2010). The pattern of Ni and Co abundances in lunar olivines. *Geochimica et Cosmochimica Acta* **74**, 784-798.

Matzen, A. K., Baker, M. B., Beckett, J. R. & Stolper, E. M. (2011). Fe–Mg partitioning between olivine and high-magnesian melts and the nature of Hawaiian parental liquids. *Journal of Petrology* **52**, 1243-1263.

Mibe, K., Fujii, T., Yasuda, A. & Ono, S. (2006). Mg-Fe partitioning between olivine and ultramafic melts at high pressures. *Geochimica et Cosmochimica Acta* **70**, 757-766.

Mysen, B. O. (2006). Redox equilibria of iron and silicate melt structure: Implications for olivine/melt element partitioning. *Geochimica et Cosmochimica Acta* **70**, 3121-3138.

Mysen, B. (2007a). Partitioning of calcium, magnesium, and transition metals between olivine and melt governed by the structure of the silicate melt at ambient pressure. *American Mineralogist* **92**, 844-862.

Mysen, B. O. (2007b). Olivine/melt transition metal partitioning, melt composition, and melt structure - Influence of $Al^{3+}$ for $Si^{4+}$ substitution in the tetrahedral network of silicate melts. *Geochimica et Cosmochimica Acta* **71**, 5500-5513.

Mysen, B. O. (2008). Olivine/melt transition metal partitioning, melt composition, and melt structure - Melt polymerization and $Q^n$-speciation in alkaline earth silicate systems. *Geochimica et Cosmochimica Acta* **72**, 4796-4812.

Nabelek, P. I. (1980). Nickel partitioning between olivine and liquid in natural basalts: Henry's law behavior. *Earth and Planetary Science Letters* **48**, 293-302.

Seifert, S., O'Neill, H. St. C. & Brey, G. (1988). The partitioning of Fe, Ni and Co between olivine, metal, and basaltic liquid: An experimental and thermodynamic investigation, with application to the composition of the lunar core. *Geochimica et Cosmochimica Acta* **52**, 603-616.

Snyder, D. A. & Carmichael, I. S. E. (1992). Olivine-liquid equilibria and the chemical activities of FeO, NiO, $Fe_2O_3$, and MgO in natural basic melts. *Geochimica et Cosmochimica Acta* **56**, 303-318.

Takahashi, E. (1978). Partitioning of $Ni^{2+}$, $Co^{2+}$, $Fe^{2+}$, $Mn^{2+}$ and $Mg^{2+}$ between olivine and silicate melts: compositional dependence of partition coefficient. *Geochimica et Cosmochimica Acta* **42**, 1829-1844.

Taura, H., Yurimoto, H., Kurita, K. & Sueno, S. (1998). Pressure dependence on partition coefficients for trace elements between olivine and coexisting melts. *Physics and Chemistry of Minerals* **25**, 469-484.

Tuff, J. & O'Neill, H. S. C. (2010). The effect of sulfur on the partitioning of Ni and other first-row transition elements between olivine and silicate melt. *Geochimica et Cosmochimica Acta* **74**, 6180-6205.

Wang, Z. & Gaetani, G. A. (2008). Partitioning of Ni between olivine and siliceous eclogite partial melt: experimental constraints on the mantle source of Hawaiian basalts. *Contributions to Mineralogy and Petrology* **156**, 661-678.

**FIGURES**

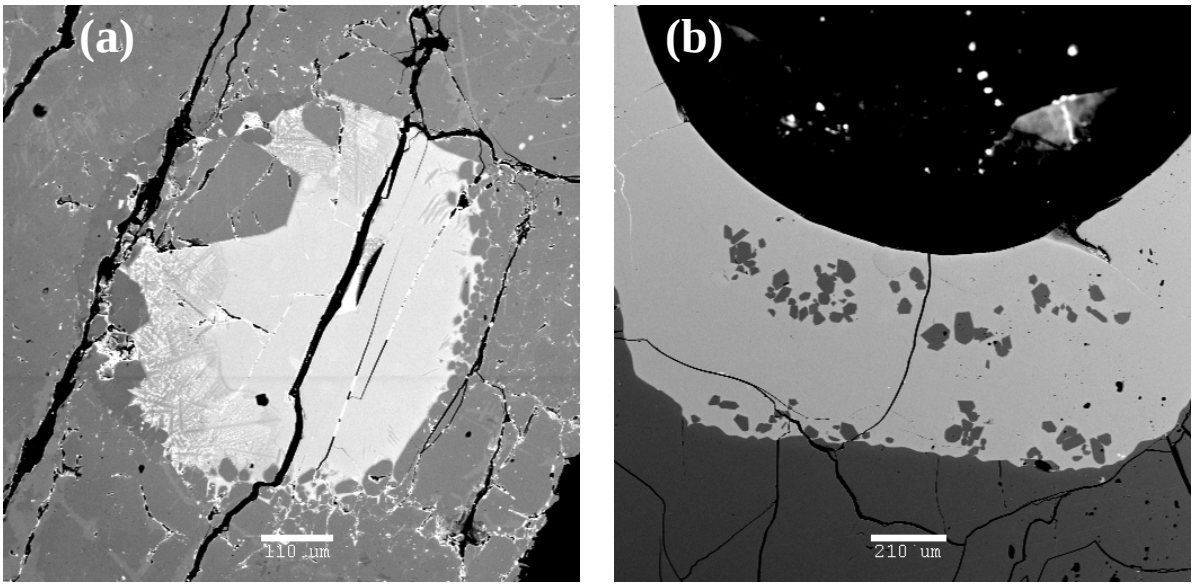


**Fig. S1.** Backscattered electron images of run products. (a) High pressure experiment (Run 13; 2.5 GPa, 1525°C): Black region in lower right-hand side of image is graphite capsule; light gray is a silicate glass (some quench crystallization is visible on left-hand side of melt pool); darker grays are olivines and low-Ca pyroxenes. Bright material filling some of the small cracks is brass from the sample mount emplaced during polishing. Scale bar is 110 μm. (b) One-atmosphere experiment (Run 25; 1-atm, 1399°C: dark gray is olivine, light gray is quenched silicate melt, and the black material at the top of the image is a void space. Scale bar is 210 μm.

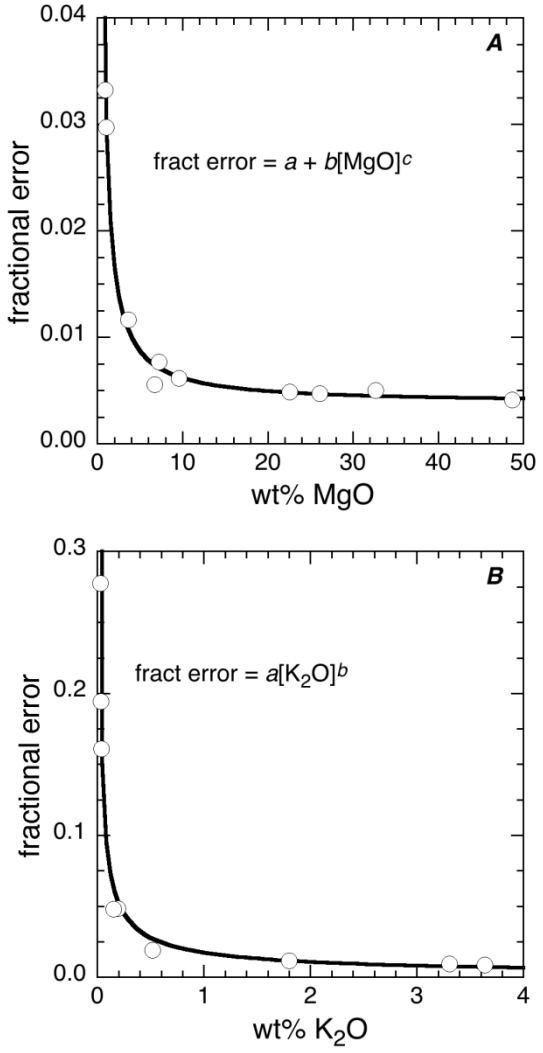


**Fig. S2.** MgO (a) and $K_2O$ (b) fractional errors (σ/mean) as a function of oxide concentration. Open circles represent fractional errors as calculated for at least 20 analyses on glass and mineral standards in the Caltech microprobe lab; analytical conditions were the same as those used for determining the major-element compositions of the experimental glasses and are described in the main text. In (A) the best-fit parameters are: ***a*** = 0.0038425, ***b*** = 0.026598, ***c*** = –1.05476; in (B) ***a*** = 0.017511, ***b*** = –0.67532; correlation coefficients for both fits are > 0.97.

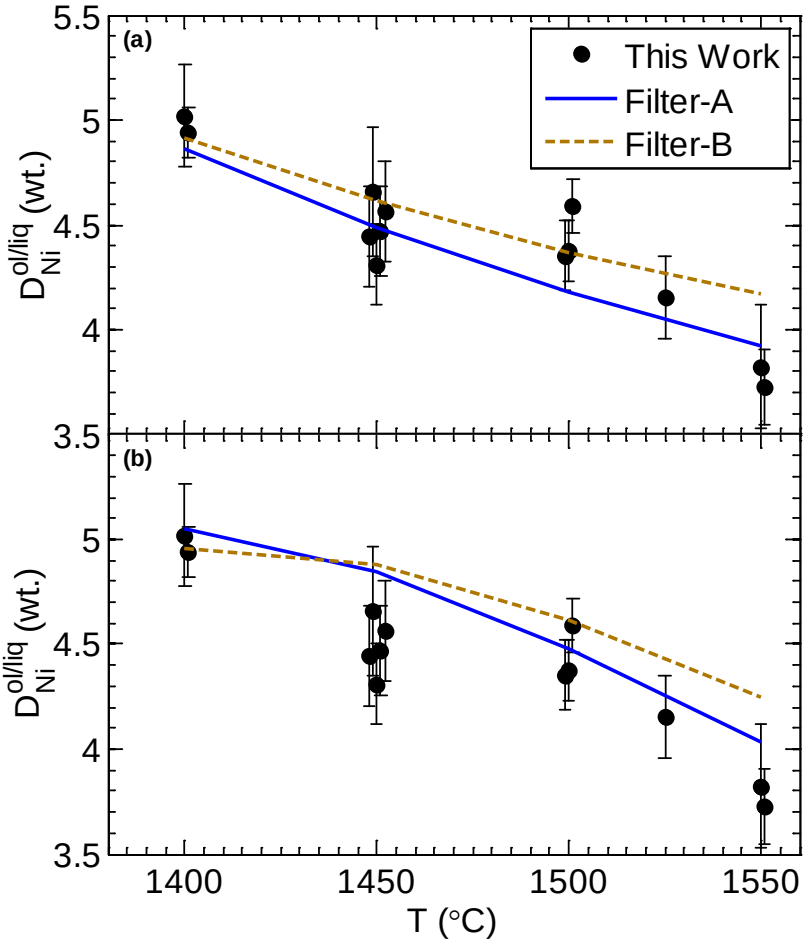


**Fig. S3.** Measured and predicted $D_{Ni}^{ol/liq}$ (by wt.) vs. temperature. In both panels of the figure, measured $D_{Ni}^{ol/liq}$ s from our experiments are shown as filled black circles with their corresponding error bars. (a) Fits using equation S4 ("regular-solution" exchange reaction). The lines correspond to the predicted $D_{Ni}^{ol/liq}$ for a liquid and olivine of constant composition (run 25) using Filter-A (solid blue) and Filter-B (dashed brown) datasets. (b) Fits using equation S5 ("regular-solution" formation reaction). Symbols and line coloring schemes as in (a)

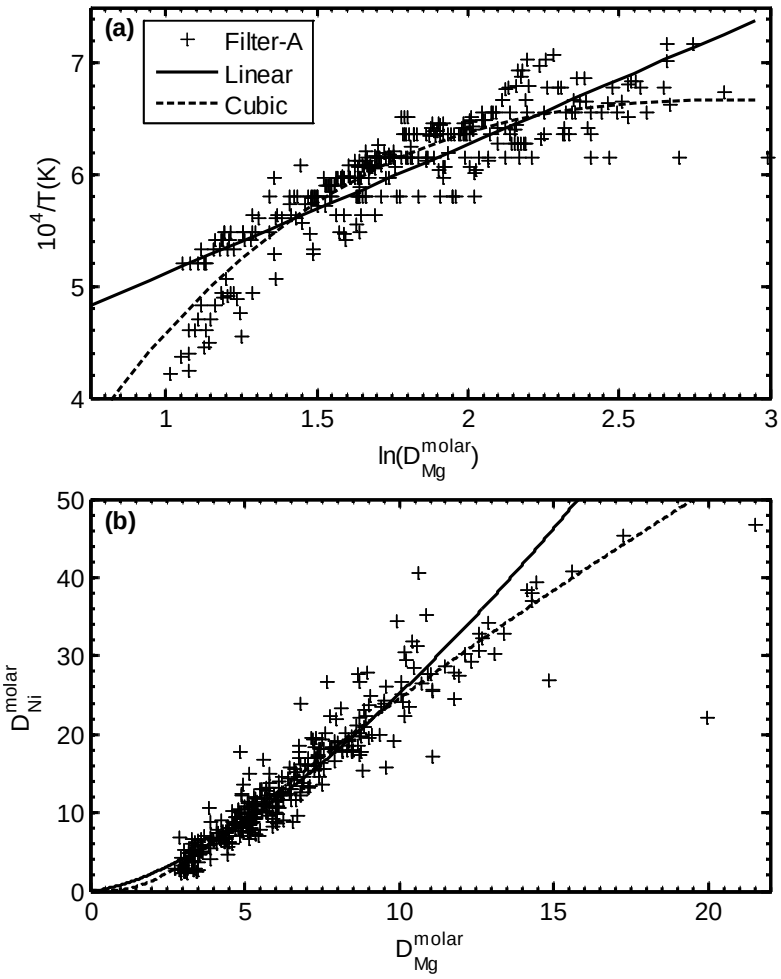


**Fig. S4** (a) Correlation between $10^4/T$(K) and ln( $D_{Mg}^{molar}$ ), where $D_{Mg}^{molar} = \frac{X_{MgSi_{0.5}O_2}^{ol}}{X_{MgO}^{liq}}$, for the Filter-A dataset. Two possible parameterizations of the observed relationship are shown: a linear least-squares fit as a solid line, and a 3rd order polynomial (cubic) least-squares fit as a dashed curve. (b) Observed and predicted variation between $D_{Ni}^{molar}$ and $D_{Mg}^{molar}$. Crosses correspond to measurements from experiments in the Filter-A dataset. Curves are predicted relationships between $D_{Ni}^{molar}$ and $D_{Mg}^{molar}$ using equation (6). For these curves, $-\frac{\Delta_{r(1)}H^{\circ}_{T_{ref},P_{ref}}}{R}$ and $\frac{\Delta_{r(1)}S^{\circ}_{T_{ref},P_{ref}}}{R}$ are taken from the fit from the Filter-A dataset using equation (5) and $1/T$ is replaced by the cubic and linear fits to the relationship between $1/T$ and $D_{Mg}^{molar}$ from panel (a).

**Table S1**. Parental/Primary Liquid Compositions

| $SiO_2$ | $TiO_2$ | $Al_2O_3$ | $Cr_2O_3$ | FeO* | MnO | MgO | CaO | $Na_2O$ | $K_2O$ | Source |
|---|---|---|---|---|---|---|---|---|---|---|
| 47.95 | 1.37 | 9.29 | 0.20 | 10.80 | 0.19 | 21.19 | 7.03 | 1.51 | 0.23 | Wright (1984) |
| 46.75 | 1.58 | 9.01 | 0.21 | 11.13 | 0.16 | 21.81 | 7.30 | 1.47 | 0.31 | Wright (1984) |
| 48.50 | 1.76 | 10.20 | 0.00 | 11.56 | 0.17 | 17.10 | 8.20 | 1.51 | 0.27 | Clague *et al.* (1991) |
| 48.46 | 2.05 | 10.72 | 0.18 | 11.27 | 0.00 | 15.76 | 9.00 | 1.85 | 0.33 | Baker *et al.* (1996) |
| 47.20 | 1.85 | 9.40 | 0.00 | 11.45 | 0.17 | 20.20 | 7.80 | 1.60 | 0.34 | Herzberg & O'Hara (2002) |
| 47.00 | 1.78 | 9.10 | 0.00 | 11.31 | 0.17 | 21.30 | 7.50 | 1.54 | 0.32 | Herzberg & O'Hara (2002) |
| 47.30 | 1.87 | 9.70 | 0.00 | 11.46 | 0.17 | 19.90 | 7.90 | 1.61 | 0.34 | Herzberg & O'Hara (2002) |
| 46.72 | 1.98 | 10.52 | 0.00 | 11.76 | 0.17 | 17.42 | 8.62 | 1.81 | 0.29 | Stolper *et al.* (2004) |
| 48.99 | 1.91 | 10.56 | 0.00 | 10.79 | 0.17 | 15.95 | 8.86 | 1.74 | 0.30 | Stolper *et al.* (2004) |
| 46.30 | 2.01 | 9.93 | 0.00 | 11.24 | 0.18 | 17.80 | 10.00 | 1.72 | 0.56 | Herzberg (2006) |
| 46.40 | 2.11 | 9.93 | 0.00 | 10.91 | 0.00 | 18.10 | 10.00 | 1.69 | 0.52 | Herzberg (2006) |
| 46.47 | 1.78 | 8.60 | 0.26 | 11.42 | 0.16 | 19.00 | 10.10 | 1.73 | 0.12 | Herzberg (2006) |
| 45.84 | 1.83 | 9.90 | 0.00 | 11.43 | 0.19 | 18.27 | 10.12 | 1.53 | 0.42 | Herzberg (2006) |
| 46.04 | 1.78 | 9.43 | 0.00 | 11.79 | 0.16 | 20.50 | 7.75 | 1.64 | 0.27 | Matzen *et al.* (2011) |
| 48.18 | 1.73 | 9.55 | 0.00 | 10.92 | 0.16 | 18.98 | 8.04 | 1.57 | 0.27 | Matzen *et al.* (2011) |
| 48.01 | 1.35 | 9.15 | 0.00 | 10.81 | 0.16 | 21.22 | 7.14 | 1.46 | 0.22 | Matzen *et al.* (2011) |
| 47.74 | 1.74 | 9.49 | 0.00 | 11.37 | 0.16 | 19.02 | 7.84 | 1.61 | 0.31 | Matzen *et al.* (2011) |
| 47.54 | 1.69 | 9.24 | 0.00 | 11.43 | 0.16 | 19.73 | 7.64 | 1.57 | 0.30 | Matzen *et al.* (2011) |

Note: All compositions listed in wt %. Zeros have been inserted for elements not calculated/reported

**Table S2**. Fit Parameters

| Reaction Fit | Dataset Used | $-\Delta_r H^{\circ}_{T_{ref},P_{ref}} / R$ (K)[a] | $\Delta_r S^{\circ}_{T_{ref},P_{ref}} / R$ | $W_{Ni\text{-}Mg}/R$ (K) | $W_{Mg\text{-}Si}/R$ (K) | $W_{Si\text{-}Ni}/R$ (K) | Mean Percent Errors of Dataset[b] Fit | Filter-B | This Work |
|---|---|---|---|---|---|---|---|---|---|
| Ex, $W_{Ni\text{-}Mg\text{-}Si}$ [c] | Filter-A | 2,942 | -2.006 | 581.1 | 3248 | 5277 | 12.9 | 12.1 | 4.0 |
| Ex, $W_{Ni\text{-}Mg\text{-}Si}$ [c] | Filter-B | 2,660 | -1.390 | -738.3 | 4906 | 6156 | 12.3 | 12.3 | 5.5 |
| Fm, $W_{Ni\text{-}Mg\text{-}Si}$ [c] | Filter-A | 5,498 | -2.582 | 581.1 | 3248 | 5277 | 13.0 | 11.5 | 6.1 |
| Fm, $W_{Ni\text{-}Mg\text{-}Si}$ [c] | Filter-B | 3,814 | -1.741 | -738.3 | 4906 | 6156 | 10.9 | 10.9 | 8.3 |

Note: For each fit, we list the reaction, the dataset used, and the resulting fit parameters.

[a] For all fit parameters, units are listed in parenthesis in the column header, where not unitless.

[b] Mean percent errors are defined as $100 \times$ (predicted $D_{Ni}^{ol/liq}$ – measured $D_{Ni}^{ol/liq}$)/measured $D_{Ni}^{ol/liq}$

[c] Simultaneous fit of Equations (S2) and (S3) as described in the text of the supplement.